Green Chemistry

PAPER

View Article Online
View Journal | View Issue

Cite this: *Green Chem.*, 2023, **25**, 8226

Bio-based captodative ligands for redox polymerization of Elium® thermoplastic composites under mild conditions†

Nicolas Giacoletto, [a] Marie Le Dot,[b] Hizia Cherif,[a] Fabrice Morlet-Savary,[b] Bernadette Graff,[b] Valérie Monnier,[c] Didier Gigmes, [a] Frédéric Dumur, [a] Hamza Olleik,[e] Marc Maresca,[e] Pierre Gerard,[d] Malek Nechab *[a] and Jacques Lalevée *[b]

Received 10th August 2023,
Accepted 4th September 2023

DOI: 10.1039/d3gc03001f

rsc.li/greenchem

Thermoplastic polymers obtained from resins such as Elium® combine desirable properties, including recyclability/reusability and excellent thermomechanical performances, at a relatively affordable cost. Nevertheless, their polymerization often requires a high amount of energy and/or involves hazardous chemical compounds. To address this last point, a series of bio-based captodative ligands was designed and synthesized in order to replace controversial phosphine oxides commonly used in low-energy initiating systems but suffering from toxicity issues. By using these captodative ligands, the curing time required for the polymerization of Elium® could be reduced from more than one hour to a mere 10 minutes. To gain a deeper insight into the redox mechanism involved during the polymerization process, the redox properties of a series of manganese(III) complexes containing different captodative ligands have been investigated employing cyclic voltammetry. It has been demonstrated that ligand exchange reactions induced by using the captodative (or push–pull) ligands possessing both electron-donating and electron-withdrawing groups had a significant impact on the reduction potential of the manganese(III) complexes. The reduction potential significantly changed depending on the type of heteroatom atom (X = O, S) and substituent included in the scaffold of the captodative ligands.

1. Introduction

Over the past 30 years, the global plastic production has seen an exponential rise, leading to environmental awareness of the negative impact of the ever-growing increase in plastic waste produced daily. Thermoset systems such as cured epoxy systems were initially implemented for the military, aeronautic, and energy sectors.[1] Thermosetting materials typically display superior strength in terms of tensile, shear, and compressive properties compared to thermoplastic ones. Despite these advantages, several drawbacks were identified concerning epoxy-based composites, including a lack of performance in terms of damage tolerance, hot/wet instability, and high manufacturing cost associated with the conventional hand-layup fabrication process.[2] Until climate change moved up to the political agenda, thermoplastics were just not worth it for high-performance engineering applications. At present, the availability of high-T_g thermoplastic materials with superior thermomechanical properties is still restricted, and the prices of these thermoplastics are often significantly higher compared to those of commercial thermoset resins.[3] In this regard, Arkema has developed novel low-viscosity resins called Elium® resins. These resins based on methyl methacrylate (MMA) chemistry display competitive thermomechanical properties compared to more established epoxy resin systems, with the formation of high-T_g polymers by the polymerization of Elium®.[4,5] The recyclability of polymerized acrylic–Elium® composites has also been demonstrated numerous times, which constitutes the strength of these Elium® resins.[6–9] On the other hand, from an economic viewpoint, a cost–benefit analysis of polymer production has revealed that thermoplastic composites produced with Elium® are 5% cheaper than those produced with epoxy resins due to reduced cycle times.[10,11] The current cost per kilogram of Elium® resin was used for

[a]*Aix Marseille Univ, CNRS, ICR UMR 7273, F-13397 Marseille, France. E-mail: malek.nechab@univ-amu.fr*
[b]*Institut de Science des Matériaux de Mulhouse IS2M, UMR CNRS 7361, F-68057 Mulhouse, France. E-mail: Jacques.lalevee@uha.fr*
[c]*Aix-Marseille Univ, CNRS, Centrale Marseille, FSCM, F-13397 Marseille, France*
[d]*GRL, Arkema, B.P. 34, F-64170 Lacq, France*
[e]*Aix-Marseille Univ, CNRS, Centrale Marseille, iSm2, F-13013 Marseille, France*
† Electronic supplementary information (ESI) available. See DOI: https://doi.org/10.1039/d3gc03001f

these calculations, which is nowadays higher than those of epoxy resins, but this cost is expected to decrease in the near future with the growth of manufacturing facilities.[11] If the sustainability of the materials is a first step toward "green" materials, the carbon footprint of the process and the chemical compound implied in the free radical polymerization of these resins are also main concerns. Thereby, the use of biosourced initiators and recyclable monomers combined with low-energy consuming polymerization will be an ideal solution. In this regard, a novel synergistic approach to initiate the polymerization of Elium® resin using a TPO (where TPO stands for 2,4,6-trimethylbenzoyl diphenylphosphine oxide) combined with a metal-based redox initiating system (RIS) was previously reported in the literature.[12] This mechanism is detailed in Scheme 1.

For strategic market applications, the access to high performance materials is a key factor. Thereby, the thermomechanical properties of the resulting polymers obtained with an organic- and a previously reported metal-based RIS[12] were investigated. Redox polymerization was performed in the absence of irradiation. The data of the performances obtained during tensile tests, DSC analysis, SEC, and Shore D are all given in Table 1.

The mechanical properties of polymers made with Elium® are drastically impacted by the initiating process. Notably, the metal-based RIS led to higher molecular weights, a twofold

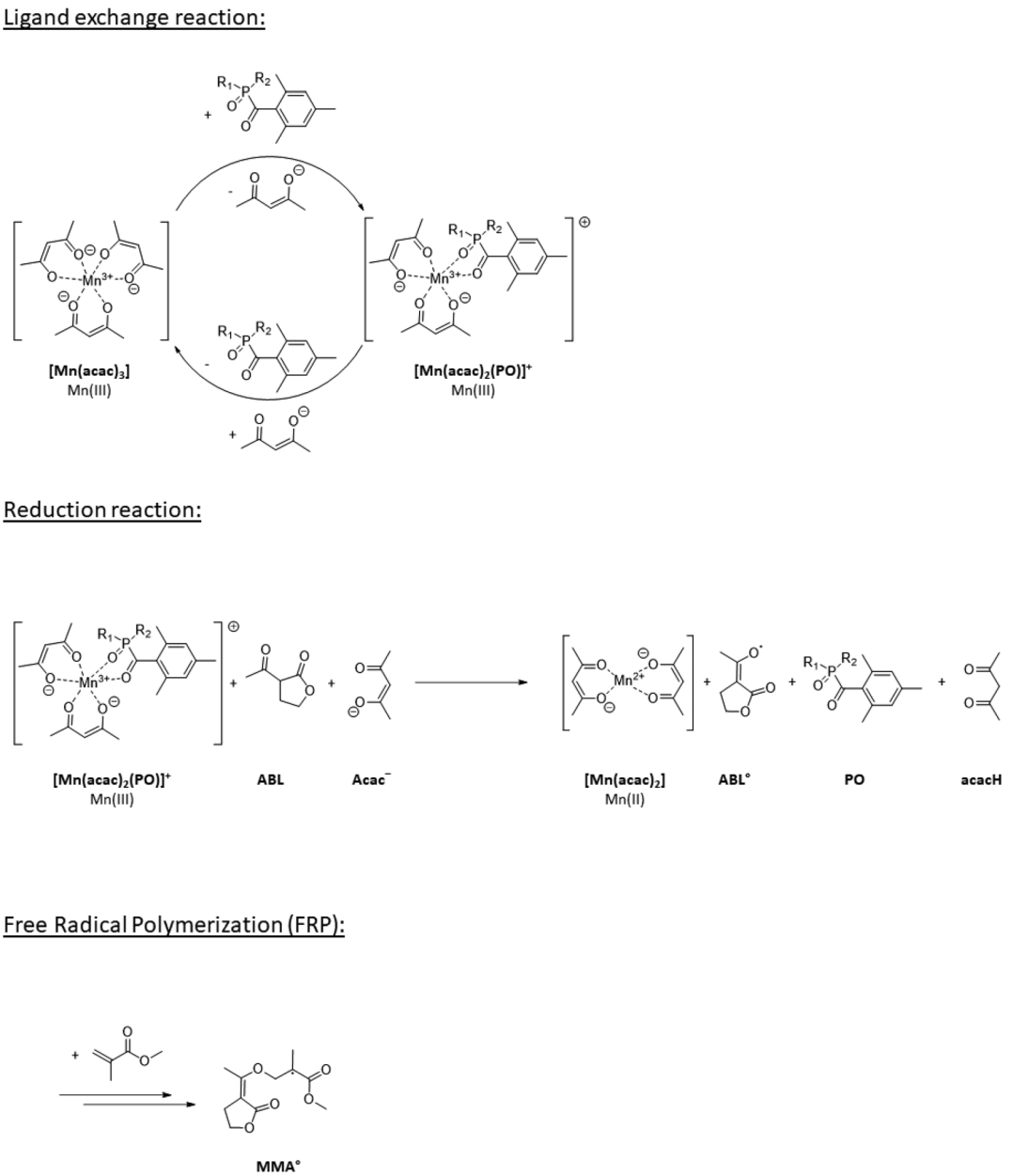

Scheme 1 Proposed chemical mechanisms for a redox free radical polymerization reaction induced by a three-component initiating system.[12]

Table 1 Final properties of Elium® thermoplastic polymers obtained with an organic-based redox initiating system formulated with 2 wt% of 2,2′-(*p*-tolylimino)diethanol and 2 wt% of dibenzoyl peroxide blend with 50 wt% tricresyl phosphate and a metal-based redox initiating system formulated with 3 wt% of TPO and 2% ABL (Scheme 1) in a first cartridge and 2 wt% of [Mn(acac)$_3$] in a second cartridge

Thermomechanical properties	Organic-based RIS	Metal-based RIS
M_n [a] (Da)	46 122	57 391
M_w [b] (Da)	212 156	238 827
Dispersity ($Đ$)	4.6	4.2
T_g (°C)	85	95
Shore D	45–55	80–90
Young's modulus (MPa)	1650	2060
Maximal stress (MPa)	38	42
Maximal strain (%)	3.5	3.3

[a] Number average molecular weight. [b] Weight average molecular weight.

higher surface hardness, a higher T_g and better performances during tensile test measurements.

However, the use of TPO-based ligands, well-known for their toxicities, is the main drawback of this strategy.[13] Therefore, our attention has turned towards new captodative ligands in order to generate new initiating radicals.[14] Captodative (or push–pull) radicals contain both electron-donating and electron-withdrawing groups, which make these radicals more stable than those with the presence of only one of these two groups. The stabilization of radicals by orbital delocalization occurs *via* a synergistic effect. Hence, this hyperconjugative stabilization is thermodynamically favorable.[15] Based on these unique properties, it was thus assumed that benzofuran substrates derived from bio-sourced salicylic esters could be excellent candidates for initiating the polymerization of methyl methacrylate-based resins.

2. Experimental section

2.1 Chemical compounds

The synthesis of the different captodative ligands is described in detail in section 3.1. In addition, all reagents and solvents were purchased from Sigma-Aldrich or Alfa Aesar and these chemicals were used as received without further purification. The different compounds were prepared with an analytical purity that met the accepted standards for new organic compounds (>98%), which was verified through high-field NMR analysis. All the other chemicals were used as received. A batch of Elium® 190 resin as well as a set of 2,2′-(*p*-tolylimino) diethanol (Dippt) and dibenzoyl peroxide blend in ~50 wt% tricresyl phosphate (BPO) were supplied by Arkema (Lacq, France). Manganese(III) tris(acetylacetonate) ([Mn(acac)$_3$]) and α-acetylbutyrolactone (ABL) were respectively provided by TCI and Sigma-Aldrich.

2.2 Evaluation of compounds' toxicity on human liver cells

The safety of the different molecules was evaluated using HepG2 cells as a model of human liver cells. Cells were routinely grown on 25 cm^2 flasks in DMEM supplemented with 10% fetal bovine serum (FBS) and 1% antibiotics (all from Thermo Fisher Scientific, Illkirch-Graffenstaden, France) in a 5% CO_2 incubator at 37 °C. For the cytotoxicity assay, cells were detached using trypsin–EDTA solution, counted using the Malassez counting chamber and seeded into 96-well cell culture plates (Greiner bio-One, Dominique Dutscher, Brumath, France) at approximately 10 000 cells per well. After 48–72 h of incubation at 37 °C to allow cells to attach and grow to confluence, wells were emptied, and cells were exposed to increasing concentrations of compounds (from 0 to 100 μM) diluted in 100 μL of a culture medium. In parallel, after 48 h of incubation at 37 °C in a 5% CO_2 incubator, cell viability was evaluated using a fluorescence assay based on resazurin (*in vitro* toxicity assay kit from Sigma-Aldrich, Lyon, France), as previously described.[16] Fluorescence values (excitation at 530 nm/emission at 590 nm) of the wells were normalized by the negative controls (cells treated with vehicle alone in DMSO) and expressed as a percentage of viability. The IC_{50} values of the compounds (*i.e.* the concentration of compounds causing a reduction of 50% of cell viability as compared to the control) were calculated using GraphPad® Prism 7 software (San Diego, CA, USA). Experiments were conducted in triplicate (n = 3).

2.3 Preparation of the two cartridges used for redox experiments

Redox initiating systems were prepared in two separated cartridges: a first cartridge with the oxidizing agent ([Mn(acac)$_3$]) and the other one containing the reducing agent (ABL) and, if mentioned, the chelating agent (bio-based captodative ligands). At the beginning of each polymerization experiment, a 1 : 1 Sulzer mixpac® mixer was used to intimately mix both cartridges. All polymerization experiments were performed under air, at room temperature, and without any purification of the Elium® 190 resin.

2.4 Electrospray ionization high-resolution mass spectrometry (HR-ESI-MS)

Manganese complexes were prepared by mixing 16 mg of a specific captodative ligand with 12 mg of the initial manganese complex [Mn(acac)$_3$] in a 300 μL solution of dichloromethane. Then, HR-ESI-MS measurements were recorded at the Spectropole (Aix-Marseille University) by using a SYNAPT G2 HDMS (Waters) mass spectrometer equipped with a pneumatically assisted atmospheric pressure (API) ionization source. Ionization of the samples was performed under the following conditions: electrospray voltage: 2.8 kV, orifice voltage: 20 V, nebulization gas flow rate (nitrogen): 100 L h^{-1}. A flight time analyser was used to obtain the HR-ESI-MS data. Measurements of the exact masses were performed in triplicate with an external calibration. In a 300 μL dichloromethane solution, the samples were diluted to 1/100 in a methanol solution with 0.01 mM sodium chloride. By infusion, the extract solutions were introduced into the ionization source at 10 μL min^{-1}.

2.5 Redox polymerization in bulk followed by optical pyrometry

For thick samples (thickness: 4.0 mm), temperature *versus* time profiles were obtained by using an Omega OS552-V1-6 industrial pyrometer. The focal distance point of the pyrometer was two-millimeter high. Both the exothermicity, as well as the gel time, defined as the time corresponding to the maximum temperature after mixing the two cartridges, could be determined.

2.6 RT-FTIR spectroscopy

The MMA function conversion was monitored using a Jasco 6600 real-time Fourier transform infrared spectrometer (RT-FTIR). The peak of the near infrared MMA C=C double bond was observed from 6096 to 6283 cm^{-1}. Rapid scan was used for fast spectral acquisition, using 1 s as the interval between scans.

2.7 Electron spin resonance (ESR)

Experiments were performed using an X-band spectrometer (Bruker EMXplus). The prepared formulations were studied in glass capillary tubes to overcome the high polarity of the Elium® resin. All experiments were performed at room temperature under air.

2.8 Cyclic voltammetry

Redox potentials were measured at room temperature in a solution of 50 : 50 v/v acetonitrile and dichloromethane by cyclic voltammetry with tetrabutylammonium hexafluorophosphate (0.1 M) as the supporting electrolyte (Voltalab 6 Radiometer; the working electrode was a platinum disk and a saturated calomel electrode (−SCE) was used as the reference; a scan rate of 0.1 V s^{-1} has been used; all potentials were determined from half-peak potentials).

2.9 Computational procedure

The enthalpies of the reactions were calculated using the uB3LYP method (base 6-31G*) and Gaussian 16 software.

2.10 Determination of Shore-D hardness

Shore D hardness measurements were performed using a digital durometer (LX-A, Huatec Group Corporation, Beijing, China), with constant load test stand (TI-D, Sauter – KERN & SOHN GmbH, Balingen, Germany), using the Shore D scale according to the CSN EN ISO 868 standard.

2.11 Determination of the glass transition temperature (T_g) by DSC analysis

The different thermal properties of the polymers obtained were monitored by DSC. The following sequence was used: first heating with 10 °C min^{-1} rate from −50 to 150 °C with 5 min of isotherm at the two extreme temperatures, then cooling with the same temperature rate and finally the second heating process, with again a heating rate at 10 °C min^{-1} from −50 to 150 °C with 5 min of isotherm. A Mettler-Toledo DSC 821e differential scanning calorimeter was used. DSC curing experiments were conducted with a dry nitrogen gas flow of 50 mL min^{-1}. The data were evaluated using STAR^e software.

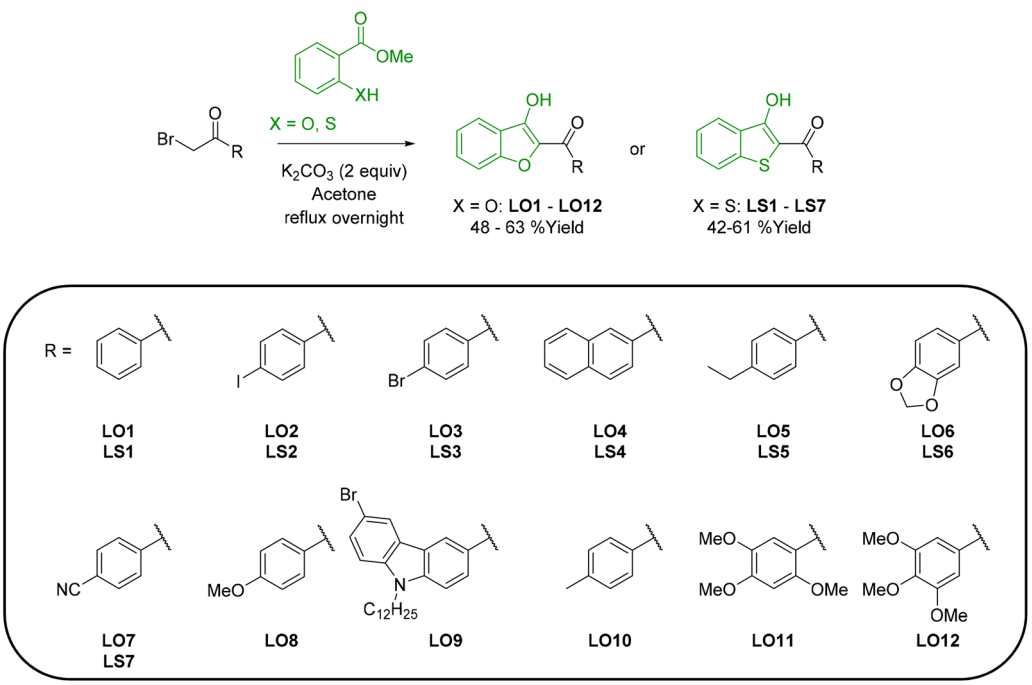

Scheme 2 New synthesized bio-based captodative ligands.

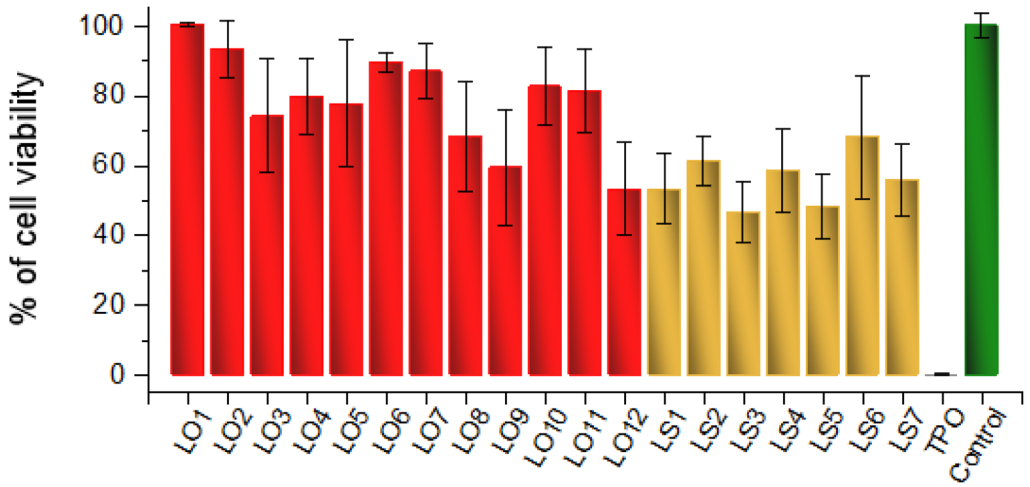

Fig. 1 Effect of **LO1–LO12**, **LS1–LS7** and TPO at 100 μM on human liver cell viability. Human liver cells (HepG2) were exposed for 48 h to 100 μM **LO1–LO12**, **LS1–LS7** or TPO before cell viability was measured using a resazurin-based assay. Results are expressed as percentage of cell viability, with cells treated with vehicle alone (DMSO) being used as a negative control, giving 100% viability (mean ± SD, n = 3).

2.12 Tensile tests

A ZwickRoell dynamometer and testXpert III software were used to perform the tensile test experiments. With an initial spacing between jaws of 25 mm, the speed spacing was fixed at 10 mm min^{-1}. To evaluate the reproducibility, a minimum of 5 specimens were studied and tested according to the DIN EN ISO 527 standard.

2.13 Size exclusion chromatography (SEC)

The samples were dissolved in tetrahydrofuran (THF) stabilized with butylated hydroxytoluene (BHT) at a concentration of 1 mg mL^{-1} and then tested at a flow rate of 1 mL min^{-1} in a custom made SEC test unit (Waters Alliance 2695 device; Waters 2414 RI and Waters 2487 Dual UV 254 nm detectors, 2 PL gel 10 μm Mixed-B, 300 × 7.5 mm columns). The SEC measurements were performed at the GRL Lacq (Arkema).

3. Results and discussion

3.1 Ligand synthesis

Salicylic acid (SA) is a phenolic pheromone that can originate from plants, making SA a bio-sourced intermediate in aspirin drug synthesis.[17] We attempted to synthesize oxygen-derived captodative ligands, starting with the methyl ester of SA. In the presence of bromoacetate, benzofuran moieties with functionalized aromatic rings were obtained in one-pot, with reaction yields ranging from 48 to 63% over two steps. The synthesis route as well as the nature of the substituent of the different captodative ligands are detailed in Scheme 2.

3.2 Evaluation of compounds' toxicity on human liver cells

To evaluate the safety of the compounds, human liver cells (HepG2) were exposed for 48 h to 100 μM **LO1–LO12**, **LS1–LS7** and TPO (ranging from 0 to 100 μM). The measurement of the percentage of cell viability demonstrated the lower toxicity of **LO1–LO12** compared to **LS1–LS7** or TPO (see Fig. 1). For **LO1–LO12** at 100 μM, the mean percentage of cell survival was 78.8%, ranging from 53.2 to 100.4% of cell viability for **LO12** and **LO1**, respectively. **LS1–LS7** at 100 μM were found to be more toxic, with a mean percentage of cell survival of 55.8%, ranging from 46.4% ± 8.8% to 68.1% ± 17.6% for **LS3** and **LS6**, respectively. TPO remained as the more toxic compound, with almost complete inhibition of cell viability at 100 μM (cell viability compared to the control).

From the results, it appears that **LO1–LO12** compounds exhibited a lower level of toxicity, with a mean IC_{50} of 304.7 μM (ranging from 102.6 to 898.3 μM for **LO12** and **LO6**, respectively). **LS1–LS7** showed higher toxicity, with a mean IC_{50} of 107.8 μM (ranging from 97.5 to 116.5 μM for **LS3** and **LS6**, respectively). TPO was found to be significantly more

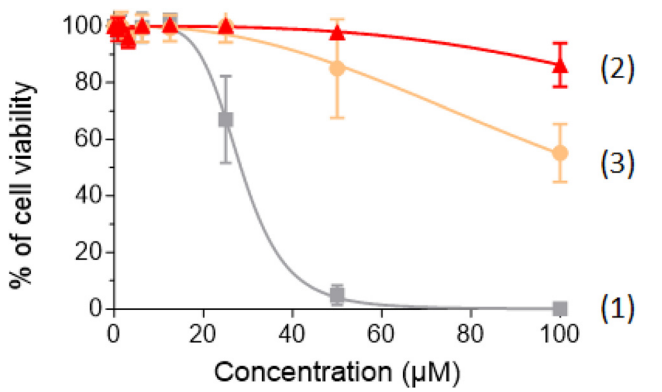

Fig. 2 Dose-dependent effects of **LO7** (curve 2, red line and symbols), **LS7** (curve 3, yellow line and symbols) and TPO (curve 1, gray line and symbols) on human liver cell viability. Human liver cells (HepG2) were exposed to increasing concentrations of **LO7**, **LS7** or TPO (ranging from 0 to 100 μM) for 48 h before cell viability was measured using a resazurin-based assay. Results are expressed as percentage of cell viability, with cells treated with vehicle alone (DMSO) used as a negative control, giving 100% viability (mean ± SD, n = 3).

toxic, with an IC_{50} value of only 28.4 μM (see the ESI, Fig. S1†). The two most efficient ligands in polymerization (**LO7** and **LS7**) were both selected and compared to TPO in order to determine their dose-dependent effects on HepG2 cells. The results are displayed in Fig. 2 to further illustrate the safer nature of **LO** and **LS** compounds compared to TPO. Even at low concentrations, a significant decrease in cell viability was observed for TPO, but not for **LO7**

3.3 Chelation and bridging ability of the new captodative ligands

Ability of the captodative ligands to chelate first-row transition metals such as manganese, iron, cobalt, nickel, zinc or cadmium is well documented in the literature.[18–20] The chelating effect comes from the two oxygen atoms acting to form dative bonds with the metal centers.[21] In parallel, many dinuc-

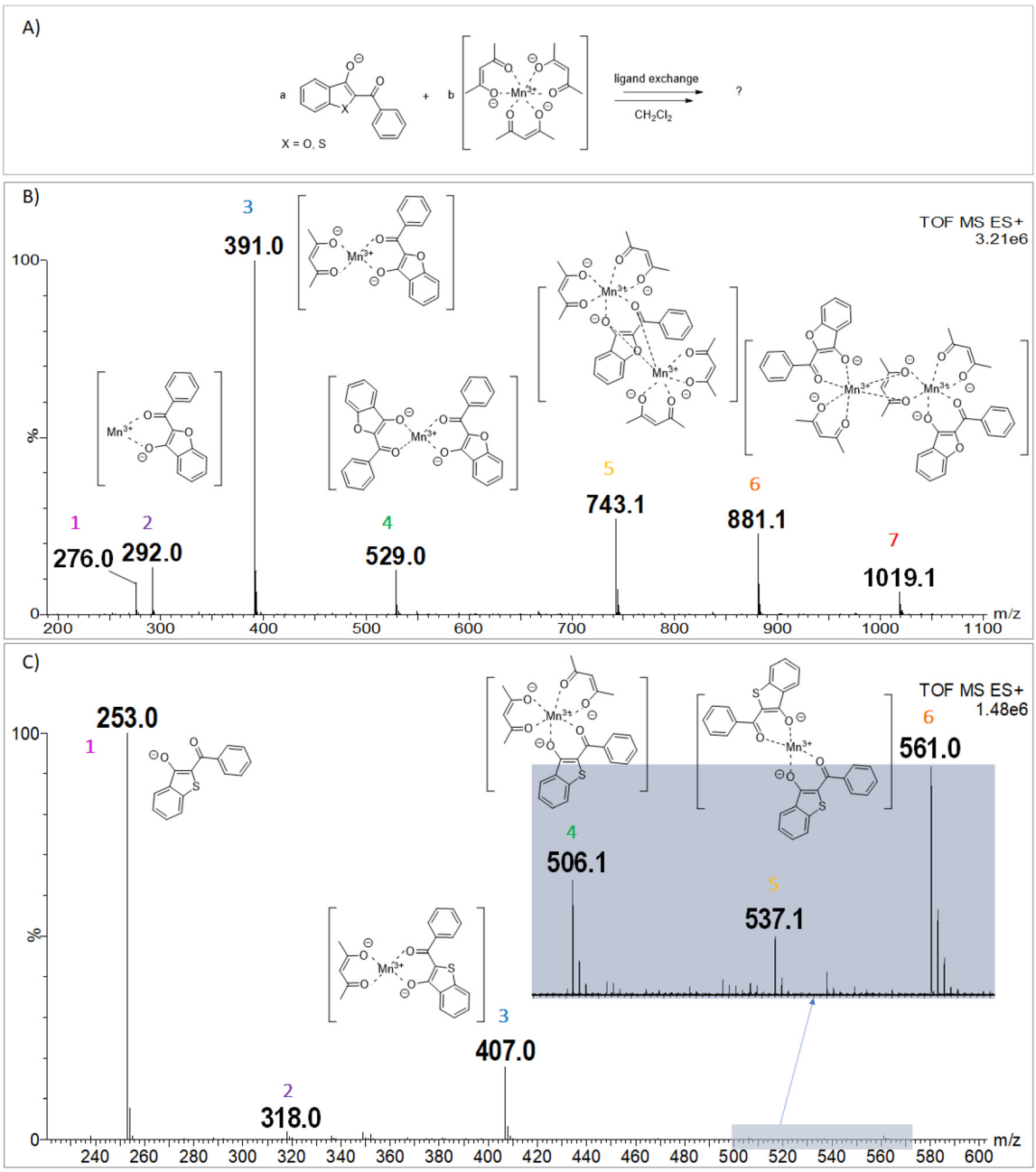

Fig. 3 (A) Schematic mechanism of ligand exchange. (B) Positive electrospray mass spectrum of ligand X = O combined with $[Mn(acac)_3]$ in CH_2Cl_2 as well as the proposed structural interpretation of the different peaks observed through the positive electrospray mass spectrum: 1: unidentified compounds, 2: [Mn(**LO1**)] = 292, 3: [Mn(acac)(**LO1**)] = 391, 4: $[Mn(\mathbf{LO1})_2]$ = 529, 5: $[Mn_2(acac)_4(\mathbf{LO1})]$ = 743, 6: $[Mn_2(acac)_3(\mathbf{LO1})_2]$ = 881, 7: unidentified compounds. (C) Positive electrospray mass spectrum of ligand X = S combined with $[Mn(acac)_3]$ in CH_2Cl_2 as well as the proposed structural interpretation of the different peaks observed through the positive electrospray mass spectrum: 1: $[Mn(acac)_2]$ = 253 or **LS1** = 253, 2: unidentified compounds = 318, 3: [Mn(acac)(**LS1**)] = 407, 4: $[Mn(acac)_2(\mathbf{LS1})]$ = 506, 5: unidentified compounds, 6: $[Mn(\mathbf{LS1})_2]$ = 561.

lear complexes have been reported in which one of the chelating ligands acts as a bridge between two metal centers.[22,23] In this context, 2-benzoyl-benzofuran-3-olate (**LO**) and 2-benzoyl-benzothiophen-3(2*H*)-olate (**LS**) were both selected to be studied by HR-MS-ESI to identify the ability of such ligands to chelate manganese atoms. Identification of the new complexes obtained by ligand exchange between the initial complex and the captodative ligand is presented in Fig. 3. In Fig. 3A, a schematic view enabling to highlight the ligand exchange reaction has been added. HR-MS-ESI spectra presented in Fig. 3B and C reveal a broad variety of new complexes, both mono- and di-nuclear, as well as the impact of the heteroatom on the diversity of the complexes obtained. In Fig. 3B, as a result of the ligand exchange reaction between **LO1** and [Mn(acac)$_3$], new metal complexes were detected: [Mn$_2$(acac)$_4$(**LO1**)] and [Mn$_2$(acac)$_3$(**LO1**)$_2$], respectively, identified at 743 Da and 881 Da as well as a mono-nuclear manganese(III) complex, [Mn(**LO1**)$_2$], identified at 529 Da. The two peaks identified at 292 Da and 391 Da are likely the result of fragmentations of mononuclear complexes. Unfortunately, the peak at 276 Da was not identified, and the one at 1019 Da could be due to the addition of two mono-nuclear manganese(III) complexes, with the previously identified [Mn(acac)(**LO1**)$_2$] and [Mn(acac)$_2$(**LO1**)] never identified as a single component. These results efficiently support the strong interaction existing between **LO1** and [Mn(acac)$_3$]. Complexes formed with the sulfur chelating ligand, **LS1**, are presented in Fig. 3C. The mono-nuclear manganese(III) complex [Mn(acac)$_2$(**LS1**)] was identified at 506 Da from the ligand exchange, and the peak at 537 Da can be attributed to the fragmentation of the [Mn(acac)(**LS1**)$_2$] complex. The peak identified at 253 Da can be attributed to **LS1** or/and [Mn(acac)$_2$], both having the exact same molecular weights. The peak at 407 Da is also probably produced from one of the two mono-nuclear manganese(III) complexes. Finally, the structure of the two peaks at 318 and 561 Da was not established. To sum up, the ability of the captodative ligands to chelate manganese metals is well evidenced by the identification of a broad range of complexes formed by ligand exchange reactions.

These new complexes formed by the ligand exchange reaction are expected to play a key role in the kinetics of free radical polymerization of Elium® thermoplastic resins.

3.4 Influence of the new complexes formed by ligand exchange on free radical polymerization (FRP) reactivity

As shown in Table 2, the different captodative ligands that have been synthesized in this work were used for the design of two- and three-component initiating systems based on a strategy previously reported.[12] As expected, no polymerization occurred with the two-component systems formed by the different captodative ligands and [Mn(acac)$_3$]. Nevertheless, after adding ABL and the captodative ligand to [Mn(acac)$_3$], a polymerization process could be detected with these three-component systems in a range of ten minutes to a couple of hours, depending on the captodative ligands used. For the first time, some captodative ligands negatively impacted the polymerization reactivity. Indeed, the time required for the polymerization was longer in the presence of captodative ligands compared to the reference system: ABL//[Mn(acac)$_3$]. From the structure–reactivity relationship, it was noticed that if all the oxygenated captodative ligands could lead to a synergistic effect (resulting in a significant increase of the reactivity compared to the reference ABL//[Mn(acac)$_3$] system), only few sulfur captodative ligands could lead to a similar effect, as exemplified with **LS6** and **LS7**. Conversely, some sulfur captodative ligands, such as **LS1** and **LS3**, severely inhibited the kinetics of polymerization. As shown in Fig. 4, four homologues were carefully chosen for a more in-depth understanding of the chemical

Table 2 Efficiency parameters of the redox initiating systems. The different systems studied were formulated with 2 wt% of ABL and 2 wt% of captodative ligands in a first cartridge and 2 wt% of [Mn(acac)$_3$] in a second cartridge. The study started when the two cartridges were mixed at t = 0

Redox initiating systems	Gel times[a] (s)	Methyl methacrylate (MMA) conversions[b] (%)	Maximal temperatures[a] (°C)	Reactivity effects[c]
ABL + **LO1**//[Mn(acac)$_3$]	1716	95–100	64	Synergistic effect (+)
ABL + **LS1**//[Mn(acac)$_3$]	5477	90	47	Inhibitory effect (−)
ABL + **LO2**//[Mn(acac)$_3$]	3326	ND	83	Synergistic effect (+)
ABL + **LS2**//[Mn(acac)$_3$]	5685	88	28	Inhibitory effect (−)
ABL + **LO3**//[Mn(acac)$_3$]	3072	ND	98	Synergistic effect (+)
ABL + **LS3**//[Mn(acac)$_3$]	6703	92	28	Inhibitory effect (−)
ABL + **LO4**//[Mn(acac)$_3$]	1399	95	81	Synergistic effect (+)
ABL + **LS4**//[Mn(acac)$_3$]	6261	93	32	Inhibitory effect (−)
ABL + **LO5**//[Mn(acac)$_3$]	2284	ND	79	Synergistic effect (+)
ABL + **LS5**//[Mn(acac)$_3$]	>7200 s	89	ND	Inhibitory effect (−)
ABL + **LO6**//[Mn(acac)$_3$]	4216	95–100	100	Synergistic effect (+)
ABL + **LS6**//[Mn(acac)$_3$]	1991	95–100	87	Synergistic effect (+)
ABL + **LO7**//[Mn(acac)$_3$]	1163	95–100	91	Synergistic effect (+)
ABL + **LS7**//[Mn(acac)$_3$]	812	ND	95	Synergistic effect (+)
ABL + **LO8**//[Mn(acac)$_3$]	3778	95–100	77	Synergistic effect (+)
ABL + **LO9**//[Mn(acac)$_3$]	2061	99	28	Synergistic effect (+)
ABL + **LO10**//[Mn(acac)$_3$]	2329	ND	91	Synergistic effect (+)
ABL + **LO11**//[Mn(acac)$_3$]	3319	86	89	Synergistic effect (+)
ABL + **LO12**//[Mn(acac)$_3$]	3181	95–100	72	Synergistic effect (+)
ABL//[Mn(acac)$_3$]	4729	98	47	Reference

ND: not determined. [a] Obtained by optical pyrometry. [b] Obtained by RT-FTIR spectroscopy. [c] Gel times compared to the reference.

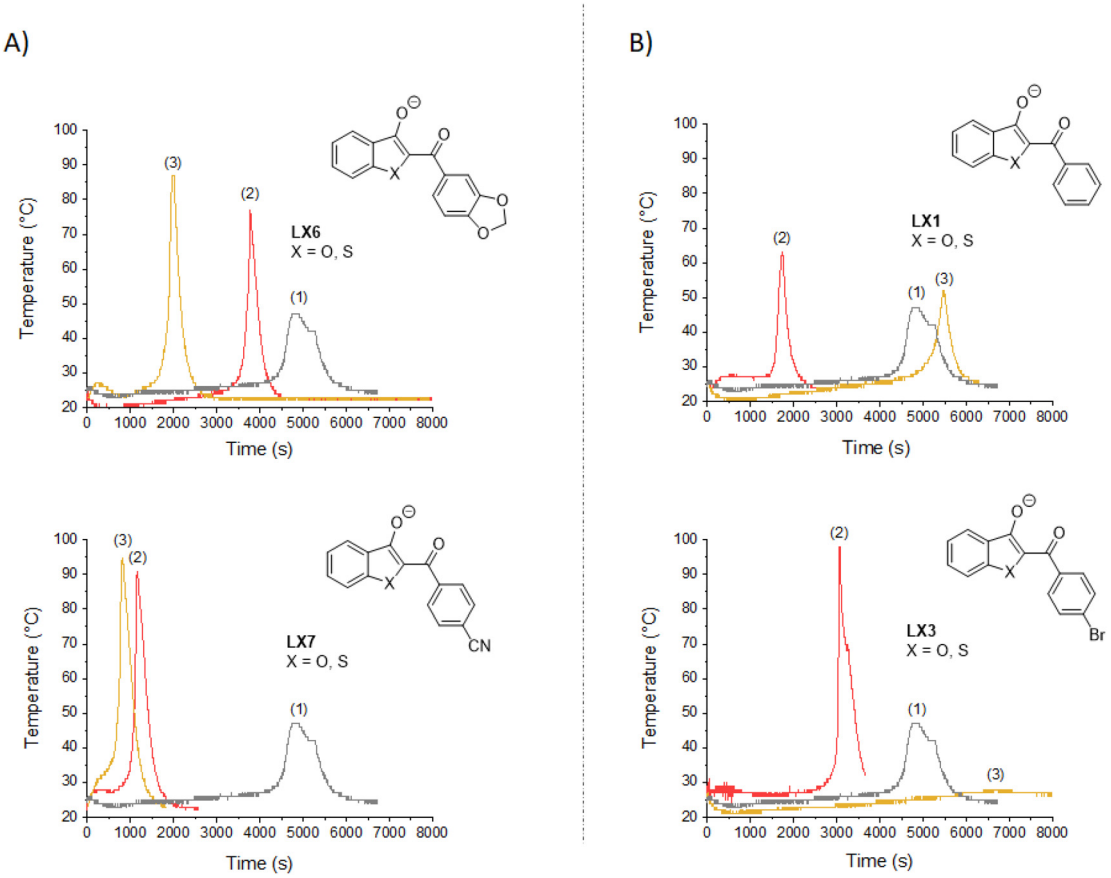

Fig. 4 Polymerization profiles (temperature *vs.* time) for a three-component redox initiating system (captodative ligands: one has an oxygen atom (X = O; curve 2, red color) and the other has a sulfur atom (X = S; curve 3, yellow color) stored in the same cartridge in comparison with ABL and, at the very last moment, mixed with the cartridge of [Mn(acac)$_3$]) compared to the initial system (cartridge 1: ABL/cartridge 2: [Mn(acac)$_3$]) (curve 1, gray color). The homologues were divided into two groups: (A) a synergistic effect in terms of reactivity was observed for both homologue captodative ligands, and (B) an opposite effect between the two homologue captodative ligands was observed, with a positive effect in terms of reactivity for the oxygenated derivatives and a negative effect for the sulfur ones.

Table 3 (A) Calculated reaction enthalpies for the reduction of the manganese(III) complexes into manganese(II) generated by mixing the initial complex, [Mn(acac)$_3$], with the different bio-based captodative ligands compared to (B) the reaction in the absence of captodative ligands

Ligands	FRP kinetic effect[a]	ΔH (kcal mol^{-1})
(A) [Mn(acac)$_2$(ligand)] + acac + ABL → [Mn(acac)$_2$] + ABL° + ligand + acacH		
LO6	Synergistic effect (+)	32.53
LS6	Synergistic effect (+)	27.35
LO7	Synergistic effect (+)	24.33
LS7	Synergistic effect (+)	29.84
LO1	Synergistic effect (+)	37.67
LS1	Inhibitory effect (−)	37.49
LO3	Synergistic effect (+)	33.90
LS3	Inhibitory effect (−)	23.47
(B) [Mn(acac)$_3$] + ABL → [Mn(acac)$_2$] + ABL° + acacH		
Acac	*x*	50.85

[a] See Table 2.

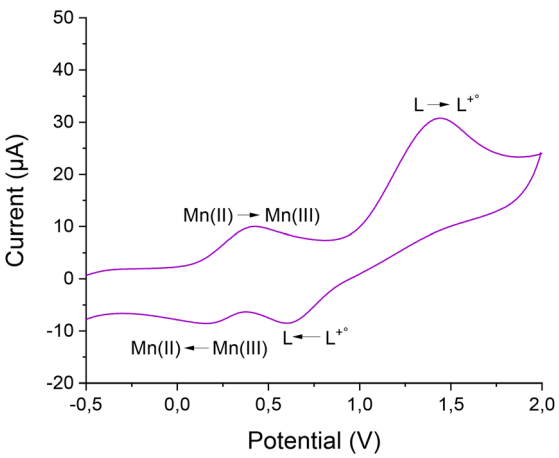

Fig. 5 Cyclic voltammogram obtained from [Mn(acac)$_3$] without any additional captodative ligands, with a special focus on the first oxido/reduction wave corresponding to the Mn(III)/Mn(II) redox reaction, and the second reduction waves attributed to the reduction of ligands in direct proximity with the metal ion center (L/L$^{+\circ}$).

mechanism. The term "homologue" in this work refers to two captodative ligands that have a similar structure, one having an oxygen atom and the other one having a sulfur atom in the heterocycle. These four homologues can be classified into two distinct categories, depending on the respective effects on the polymerization kinetics: (A) **LX6** and **LX7**, for which a synergistic effect in terms of reactivity was observed for both homologue captodative ligands; and (B) **LX1** and **LX3**, for which an opposite effect in terms of reactivity was determined for two homologue captodative ligands.

Table 4 Electrochemical data for the blend of **LO** or **LS** with [Mn(acac)$_3$] induced by the ligand reaction between the captodative ligands and the initial [Mn(acac)$_3$] complex

	Redox reactions									
	Metal redox reaction (Mn(III)/Mn(II))					Ligand redox reaction (L/L$^{+\circ}$)				
Blends	E_{pa} (V)	E_{pc} (V)	$E_{1/2}$ [a] (V)	ΔE [b] (mV)	I_{pc}/I_{pa}	E_{pa} (V)	E_{pc} (V)	$E_{1/2}$ [a] (V)	ΔE [b] (mV)	I_{pc}/I_{pa}
[Mn(acac)$_3$]/**LO6**	0.16	0.43	0.38	270	3.9	1.25	1.11	1.2	140	1.0
[Mn(acac)$_3$]/**LS6**	0.15	0.39	0.3	240	5.3	1.35	1.16	1.3	190	8.3
[Mn(acac)$_3$]/**LO7**	0.22	0.48	0.4	260	0.6	1.28	1.05	1.2	230	3.7
[Mn(acac)$_3$]/**LS7**	0.19	0.52	0.4	330	0.3	1.49	1.32	1.4	170	4.9
[Mn(acac)$_3$]/**LO1**	0.08	0.47	0.3	390	1.5	1.41	0.58	1.0	830	7.2
[Mn(acac)$_3$]/**LS1**	−0.05	0.41	0.2	460	1.3	1.37	−0.05	0.7	1420	3.5
[Mn(acac)$_3$]/**LO3**	0.10	0.50	0.3	400	2.8	1.35	0.59	1.0	760	13.5
[Mn(acac)$_3$]/**LS3**	−0.28	0.48	0.1	760	1.0	1.46	−0.29	0.6	1750	4.0
[Mn(acac)$_3$]	0.16	0.43	0.3	270	3.5	1.44	0.56	1.0	880	12.0

[a] $E_{1/2} = ((E_{pc} + E_{pa})/2)$. [b] $\Delta E = |E_{pc} - E_{pa}|$.

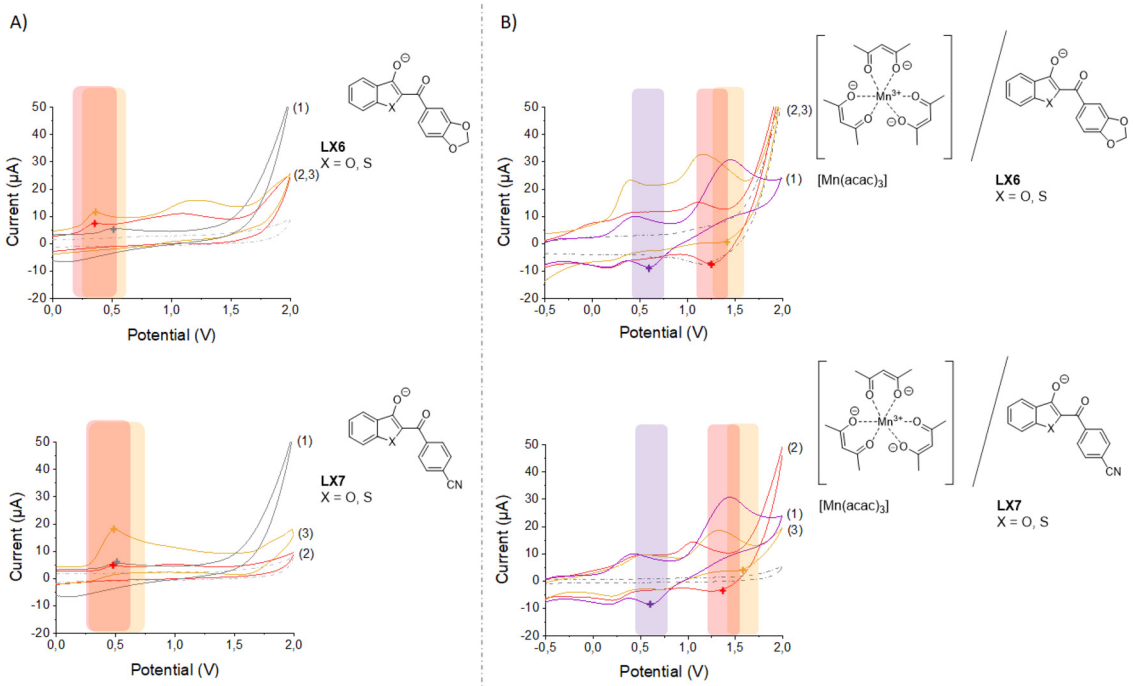

Fig. 6 Two couples (**LX6** and **LX7**) of homologue captodative ligands showing synergistic effects (gain of reactivity when combined with ABL and [Mn(acac)$_3$]) were selected and further investigated by cyclic voltammetry. (A) Cyclic voltammograms of bio-based captodative ligands in their free form (without the presence of manganese complexes) and (B) in their chelated form (in the presence of manganese complexes). The homologue with an oxygen atom (X = O; red color) is shown in curve 2, and the one with a sulfur atom (X = S; yellow curve) in curve 3, and the reference, ABL, is shown in curve 1 (gray curve). Later, both homologues were tested in the presence of [Mn(acac)$_3$] to evaluate the effects of captodative ligands on the reduction potential of manganese complexes. The homologue with an oxygen atom (X = O; red curve) is shown in curve 2, the one with a sulfur atom (X = S; yellow curve) in curve 3, and the reference [Mn(acac)$_3$] alone is shown in curve 1 (purple curve).

The gel time, final conversion and exothermicity monitored during the polymerization initiated by each captodative ligand studied in association with ABL and [Mn(acac)$_3$] are summarized in Table 2 and compared to the reference ABL//[Mn(acac)$_3$] combination in order to identify the contribution of the captodative ligands on the initiating systems. The gain value observed for the gel time was calculated using eqn (1).

$$\% \text{ increase} = ((\text{new value} - \text{reference value})/\text{reference value}) \times 100 \quad (1)$$

The reference value corresponds to the gel time obtained for the ABL//[Mn(acac)$_3$] system. For example, ligand **LS3** increased by 42% the time required to start the polymerization (negative effect) compare to the reference system. In the case of **LO3**, which is the oxygenated homologue of **LS3**, the gel time decreased by 35% (positive effect). The best kinetics were obtained for **LO7** and **LS7**, which are both homologues in terms of chemical structures with, respectively, an oxygen and a sulfur heteroatom. The gain value obtained upon the gel time compared to the reference was around 75% and 83%, respectively.

After determining the impact of the captodative ligands on the polymerization reactivity, the objectives were then identifying the critical properties of these new complexes formed by ligand exchange that were responsible for the enhancement or the decrease in reactivity of the three component initiating systems compared to the reference ABL//[Mn(acac)$_3$] system.

3.5 Structure–reactivity relationship: cyclic voltammetry and molecular modeling investigations

Reduction reactions of the manganese complexes formed by mixing the initial complex [Mn(acac)$_3$] with the benzofuran ligands derived from bio-sourced salicylic esters were evaluated by molecular modelling. Reaction enthalpies (ΔH) obtained for the different complexes are summarized in Table 3. The reduction of the different manganese(III) complexes obtained by mixing [Mn(acac)$_3$] with the different captodative ligands highlights that [Mn(acac)$_2$(**LX**)] should be more favorable to be reduced (reduction A: $\Delta H \ll 50.85$ kcal mol^{-1}) than the initial complex [Mn(acac)$_3$] (reduction B: ΔH = 50.85 kcal mol^{-1}), which is coherent with most of the experimental results shown in Fig. 4, but this does not mean that some sulfur captodative ligands negatively impact the kinetics of polymerization.

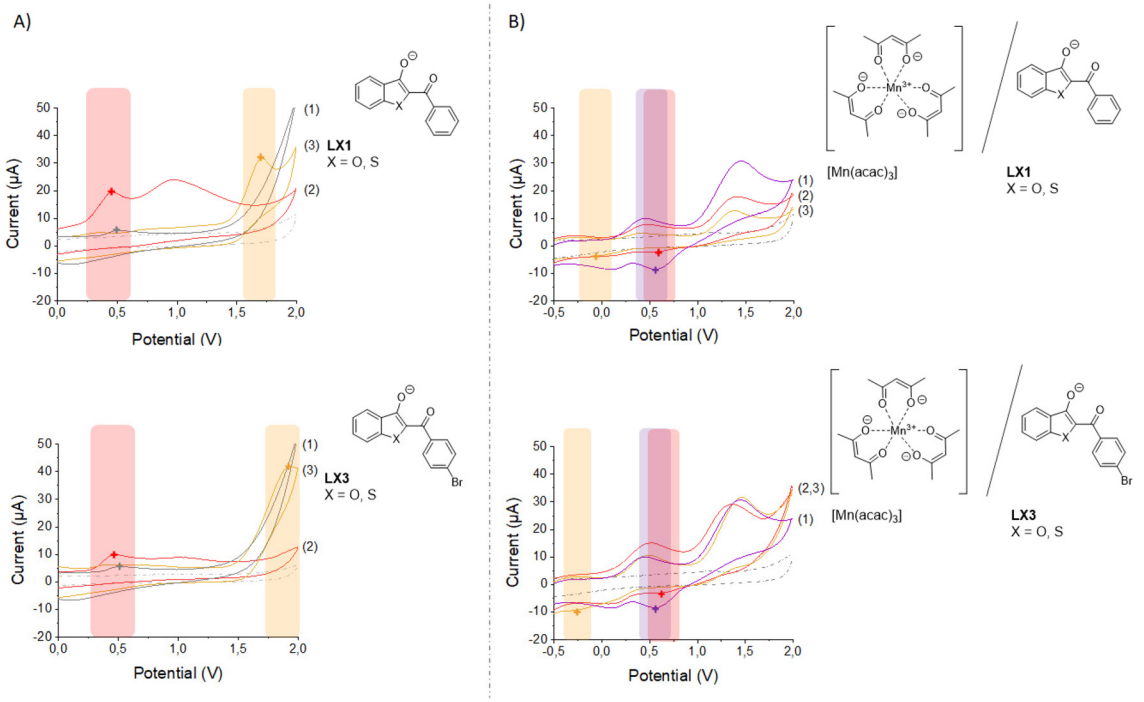

Fig. 7 Two couples (**LX1** and **LX3**) of homologue captodative ligands having "opposite" effects (the oxygenated ones lead to a synergistic effect on polymerization reactivity when combined with ABL and [Mn(acac)$_3$] and the sulfur ones behave as an inhibitor when combined with ABL and [Mn(acac)$_3$]) were selected and further investigated by cyclic voltammetry. (A) Cyclic voltammograms of bio-based captodative ligands in their free form (without the presence of manganese complexes) and (B) in their chelated form (in the presence of manganese complexes). The homologue with an oxygen atom (X = O; red color) is shown in curve 2, the one with a sulfur atom (X = S; yellow curve) in curve 3, and the reference, ABL, gray curve is shown in curve 1. Later, both homologues were tested in the presence of [Mn(acac)$_3$] to evaluate the effects of captodative ligands on the reduction potential of manganese complexes. The homologue with an oxygen atom (X = O; red curve) is shown in curve 2, the one with a sulfur atom (X = S; yellow curve) in curve 3, and the reference [Mn(acac)$_3$] alone is shown in curve 1 (purple curve).

In addition to the enthalpy calculations, cyclic voltammetry experiments have been carried out on manganese(III) complexes in the presence of captodative ligands in order to identify the effects of the captodative ligands on reduction potentials. In line with other reports,[24–26] the idea is to correlate the redox potential of these complexes with their reactivities (synergistic or inhibitory effects) observed in redox free radical polymerization. Previous research[24] on the cyclic voltammetry of coordinated manganese(III) with halogen ligands has shown that these new complexes display a one electron quasi-reversible oxidation wave corresponding to the manganese(II)/manganese(III) redox couple and a second signal detected at a more anodic potential assigned to the redox reaction of the ligands chelated to the metal ion center ($L/L^{+\circ}$). The two different signals detected at anodic potentials are presented in Fig. 5.

Electrochemical data obtained during the cyclic voltammetry study are summarized in Table 4. A special focus on the second redox reaction ($L/L^{+\circ}$) wave is highlighted, and the intrinsic oxido-reduction properties of the captodative ligands are summarized in Fig. 6 and 7.

To quantitatively assess the effect of the captodative ligands on the redox potentials of the manganese(III) complexes, the intrinsic redox potentials of these ligands were assessed as shown in Fig. 6A and 7A. All the captodative ligands that have a positive effect on the kinetics of the free radical polymerization of Elium® exhibit a cathodic potential at 0.5 V. Conversely, in the case of **LS1** and **LS3**, where the polymerization was inhibited by these ligands, higher cathodic potentials were determined, ranging between 1.5 V and 2 V.

After studying the intrinsic redox properties of the captodative ligands in the absence of manganese complexes, the investigation of the complexes induced by ligand exchange reactions when captodative ligands were in the presence of [Mn(acac)$_3$] revealed a strong correlation between the intrinsic redox potential of the ligand-centered events ($L/L^{+\circ}$) and the effect on the kinetics of the free radical polymerization of Elium®. The first irreversible waves corresponding to the Mn(III)/Mn(II) redox reaction present similar cathodic peak potentials for all the different complexes studied. Conversely, the second wave corresponding to the conjugated ligand redox reaction ($L/L^{+\circ}$) looks easier to correlate with the kinetic effect than the first wave corresponding to the Mn(III)/Mn(II) redox reaction. Indeed, for the captodative ligands that enhance the kinetic reaction (synergistic effect) of the free radical polymerization of Elium® resins, the cathodic peak potential as well as

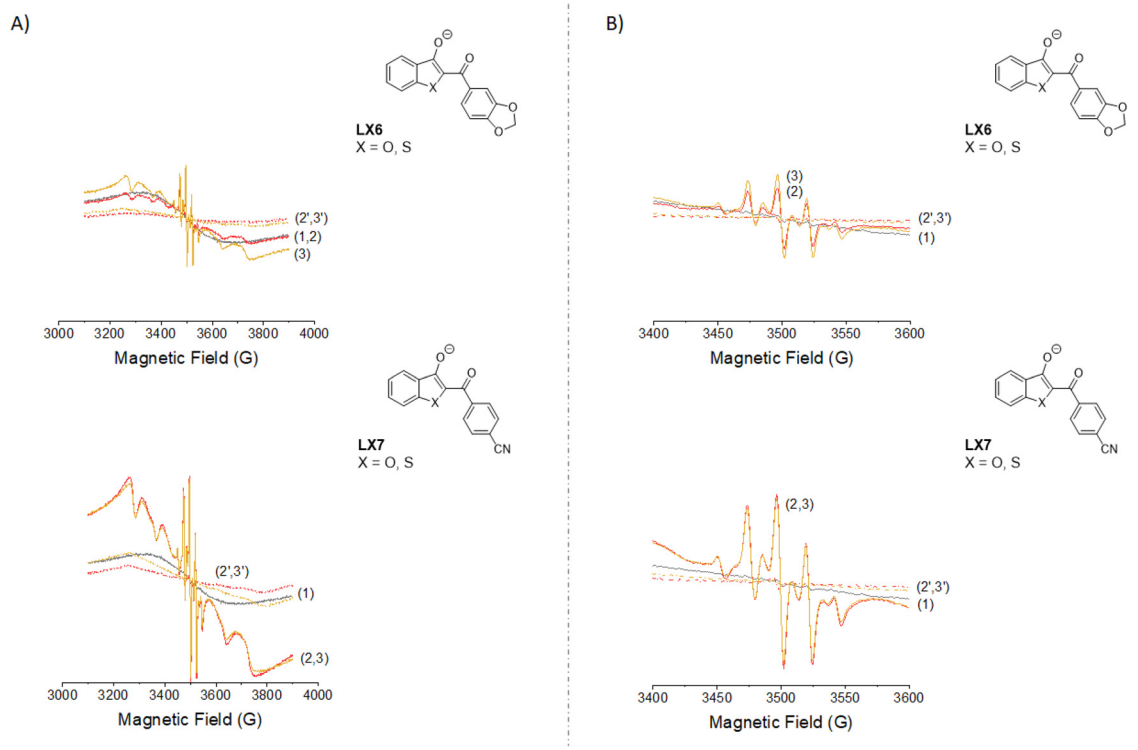

Fig. 8 Two couples of homologue captodative ligands showing synergistic effects on the free radical polymerization of Elium® were selected and further investigated by ESR experiments. (A) The experimental ESR spectrum of manganese(II) apparition initiated by the redox initiating system and (B) long-lived (macro-)radicals generated from the polymerization of MMA monomer in the presence of PMMA were monitored to evaluate the effect of captodative ligands in a redox initiating system to generate long-lived (macro-)radicals from MMA. In parts (A) and (B), the initial redox initiating system (ABL/[Mn(acac)$_3$]) is shown in curve 1, gray color, then the homologue with an oxygen atom (X = O; curve 2; red color) and the one with a sulfur atom (X = S; curve 3; yellow color); these were added to the initial redox initiating system (ABL/[Mn(acac)$_3$]). The curves 2′ (X = O; dash dot red color) and 3′ (X = S; dash dot yellow color) were added to attest to the inefficiency of the captodative ligands to reduce the metal complex in the absence of ABL.

the half-wave potential are higher than those of the initial complex [Mn(acac)$_3$] (E_{pc} > 0.56 V). To conclude on the structure–reactivity–efficiency relationship, manganese complexes induced by ligand exchange in the presence of synergistic captodative ligands are better oxidizing agents due to their higher cathodic peak potential. Conversely, the ones that negatively affect the kinetic reaction present cathodic potential peaks significantly lower than the initial complex ($E_{pc} \ll$ 0.56 V). To sum up, thanks to this study, the narrow redox potential window for which manganese complexes reflect the possibility of improving the redox polymerization of Elium® has been established. The synthesis of bio-based captodative ligands and the deepest understanding of the structure–reactivity–efficiency relationship allow the possibility in the near future to fine-tune redox potentials *via* ligand modifications, expanding upon the limited highly efficient redox initiating systems for the free radical polymerization of Elium® resins.

3.6 Effect of captodative ligands on the reduction reaction of the manganese complex

In addition to the electrochemical data obtained from cyclic voltammetry, as shown in Fig. 8A and 9A, ESR experiments were performed in order to monitor the manganese(II) generated from the reduction of manganese(III) complexes in the presence and absence of ABL, and then in the presence and absence of captodative ligands, and finally in the presence of both ABL and captodative ligands. Once again, the four different captodative ligand homologues were divided into two groups. In Fig. 8, it is seen that both homologues have a synergistic effect on the reactivity of the free radical polymerization of Elium®, and in Fig. 9, it is seen that the oxygenated ligands have a positive effect on the reactivity when the sulfur ones have an inhibitory effect. More specifically, Fig. 8A and 9A show that the presence of manganese(II) (the reduced form of manganese(III) acetylacetonate) was monitored by ESR experiments in Elium® 190 resins in a magnetic field range of 3100 and 3900 G. Mn^{2+} (I = 5/2) is a paramagnetic species and therefore ESR-active, while diamagnetic Mn^{3+} (I = 2) is not active and thus ESR-silent.[27] The Mn^{2+} ESR-active form exhibits a distinctive six-band spectrum. As shown in Fig. 8, homologues with synergistic effects for both captodative ligands were studied in a three-component configuration. In this configuration, the hyperfine structure of Mn^{2+} was identified for both captodative ligands (X = O, curve 2, red curve, and X = S, curve 3, yellow curve) in the presence of ABL and [Mn(acac)$_3$]. Moreover, the initial system ABL and [Mn(acac)$_3$] (curve 1, gray

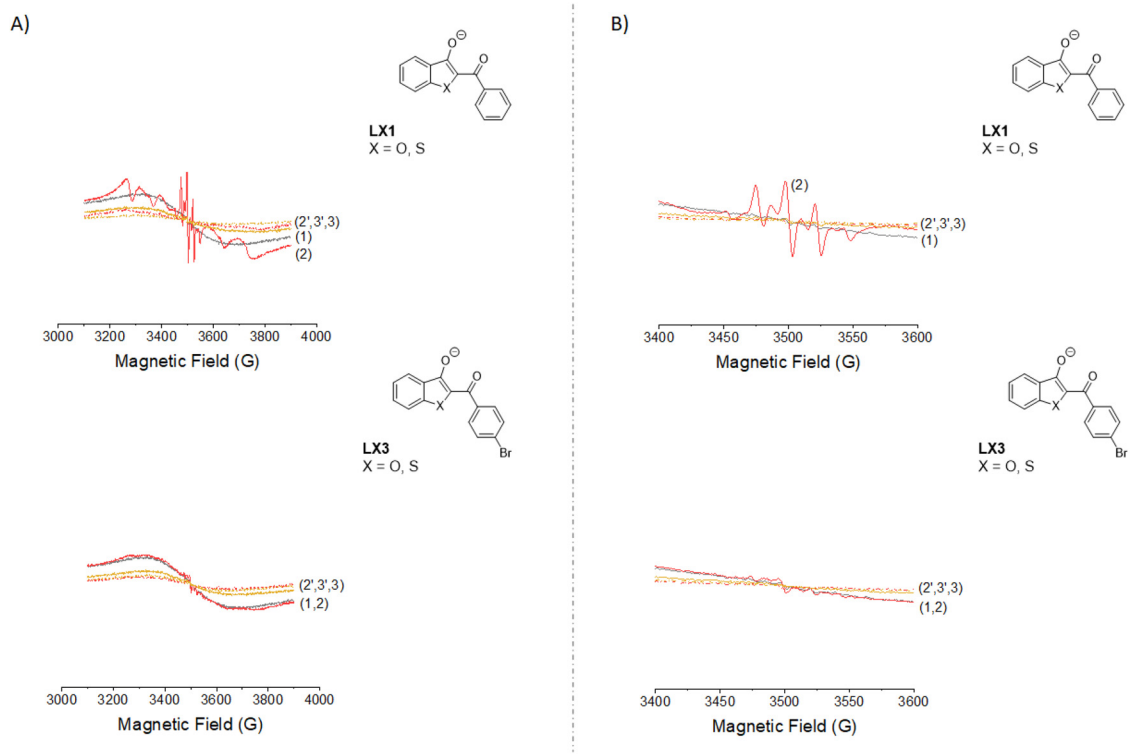

Fig. 9 Two couples (**LX1** and **LX3**) of homologue captodative ligands having "opposite" effects (the oxygenated ones lead to a synergistic effect on the polymerization reactivity when combined with ABL and [Mn(acac)$_3$] and the sulfur ones behave as an inhibitor when combined with ABL and [Mn(acac)$_3$]) were selected and further investigated by ESR experiments. (A) The experimental ESR spectrum of manganese(II) apparition initiated by the redox initiating system and (B) long-lived (macro-)radicals generated from the polymerization of MMA monomer in the presence of PMMA were monitored to evaluate the effect of captodative ligands in the redox initiating system. In parts (A) and (B), the initial redox initiating system (ABL/[Mn(acac)$_3$]) is shown in curve 1, gray color, then the homologue with an oxygen atom (X = O; curve 2; red color), and the one with a sulfur atom (X = S; curve 3; yellow color); these were added to the initial redox initiating system (ABL/[Mn(acac)$_3$]). The curves 2′ (X = O; dash dot red color) and 3′ (X = S; dash dot yellow color) were added to attest to the inefficiency of the captodative ligands to reduce the metal complex in the absence of ABL.

curve) leads to a broadband in the characteristic range of Mn^{2+}. Contrastingly, as expected, no evidence of Mn^{2+} was highlighted in a two-component configuration involving the captodative ligand (X = O, curve 2′, dash dot red curve, or X = S, curve 3′, dash dot yellow curve) mixed with [Mn(acac)$_3$]. To sum up, if the chelation and bridging abilities of the new captodative ligands are clearly established, as shown in Fig. 3, it can be seen that the reduction of Mn^{3+} into Mn^{2+} is possible only in the presence of ABL (curves 1, 2 and 3). Therefore, the role of ABL as a reducing agent is clearly defined. Even though the presence of captodative ligands affects the ability of the metal complexes to be reduced (Fig. 6 and 7), the finalization of the mechanistic study was done by monitoring the appearance of the propagating radicals PMMA° and MMA°. The characteristic signature of these long-lived macroradicals/radicals in polymeric matrices was shown in a previous report,[12] with a specific signal in a magnetic field range of 3400 and 3600 G. The results are shown in Fig. 8B. A correlation can be clearly established between the appearance of Mn^{2+} and the amount of long-lived PMMA° and MMA° generated.

As shown in Fig. 9, homologues with opposite effects were studied in a three-component configuration. Two-component configurations in the absence of ABL are also presented (X = O, curve 2′, dash dot red curve, and X = S, curve 3′, dash dot yellow curve), but they do not lead to any polymerization because the reducing agent is missing when the captodative ligands are mixed with [Mn(acac)$_3$]. Thereby, the two-component configuration based on ABL (reducing agent) and [Mn(acac)$_3$] (oxidizing agent) is used as a reference (curve 1, gray curve). In this present work, kinetic effects are expected to be correlated to the amount of manganese(II) generated by the reduction of the manganese(III) complex (Fig. 9A) as well as the amount of long-lived radicals detected (Fig. 9B). **LS1** and **LS3** negatively impact the polymerization time, unlike **LO1** and **LO3**, their respective homologues (see Fig. 4). In a three-component system (X = O, curve 2, red curve, and X = S, curve 3, yellow curve), both **LS1** and **LS3** lead to a lower amount of manganese(II) generated compared to **LO1** and **LO3** (see Fig. 9A). The amount of manganese(II) is in good agreement with the better oxidizing nature of chemicals generated by ligand exchange (see Fig. 7). The reducing reaction is the most crucial step because it will generate, in parallel with manganese(II), radicals susceptible to initiating the polymerization of Elium®. In this connection, both **LS1** and **LS3** lead to lower amounts of long-lived radicals generated compared to **LO1** and **LO3**.

3.7 Proposed chemical mechanisms for the three-component initiating system

The chelating ability of the captodative ligands was demonstrated by HR-ESI-MS by identifying a diverse range of mono- or di-nuclear complexes induced by ligand exchange reactions from the captodative ligand studied and [Mn(acac)$_3$]. These complexes can be generalized under the formula [Mn$_x$(acac)$_y$(LX)$_z$] and they exhibit different cathodic peak

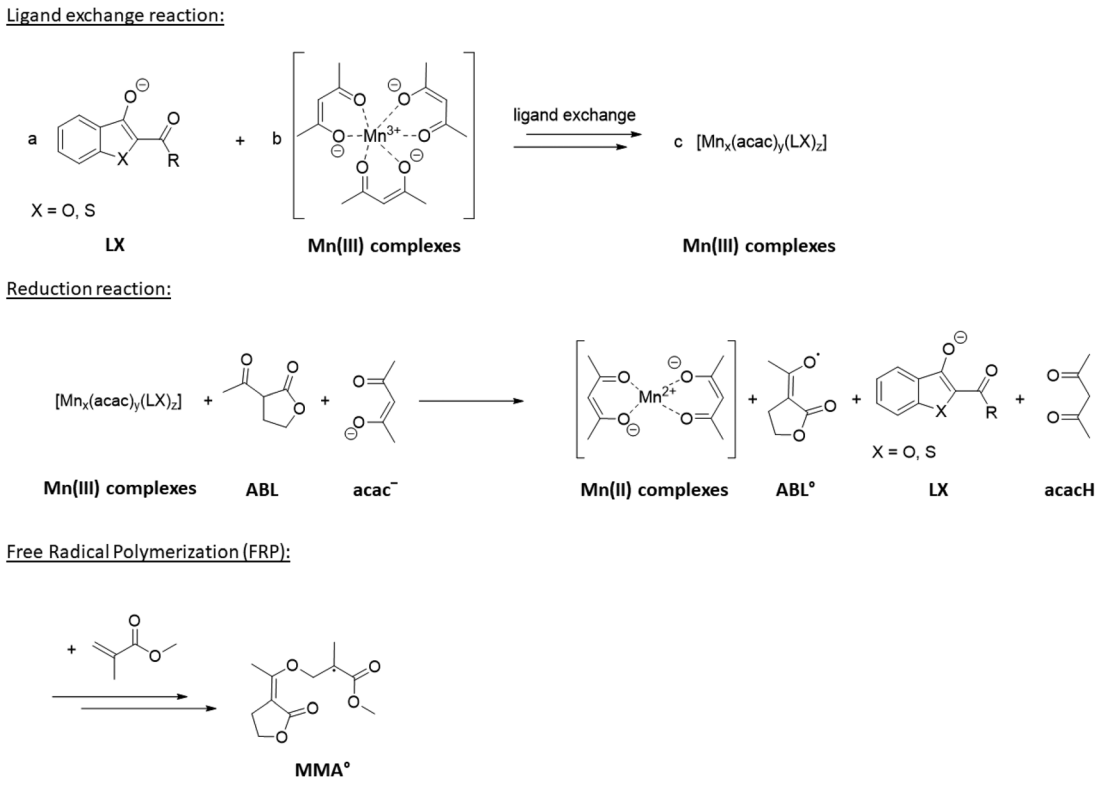

Scheme 3 Proposed chemical mechanisms for redox free radical polymerization using captodative ligands in a three-component initiating system.

potentials compared to the initial [Mn(acac)$_3$]. As a consequence, depending on the substituent and the heteroatom present in the scaffold of captodative ligands, new complexes generated by ligand exchange can be qualified as "better" or "worse" oxidizing agents compared to [Mn(acac)$_3$]. Based on the metal acetylacetonate–bidentate ligand interaction mechanism, if captodative ligands are good chelating agents, they do not induce the reduction of manganese(III) into manganese(II). Thereby, captodative ligands were combined with ABL, used in a three-component system as a reducing agent, in order to generate radicals capable of initiating the polymerization of Elium®. A proposed mechanism is displayed in Scheme 3.

4. Conclusion

Bio-based captodative ligands were successfully synthesized, and all of them exhibit a significantly lower toxicity toward human liver cells (HepG2) than TPO. In addition, most captodative ligands can be used in combination with ABL and [Mn(acac)$_3$] to broaden the limited range of redox initiating systems suitable for the free radical polymerization of Elium® resins. Furthermore, the use of captodative ligands in a three-component redox system can efficiently regulate the open time of the redox polymerization from 10 min to 2 hours, depending on the captodative ligand used. As a consequence, the polymerization of Elium® resins is perfectly suitable for high-speed industrial composite lines or, conversely, applications requiring long open times, such as joints applied to aeronautic parts, for example. The last but not least objective pursued in this study was to quantify the effects of ligands on the redox potential of manganese complexes obtained from ligand exchange. The aim was, thereby, to establish a structure–reactivity–efficiency relationship in three-component redox initiating systems. Manganese complexes with captodative ligands improve the kinetic reactions of the free radical polymerization of Elium® resins and exhibit cathodic peak potentials higher than the initial complex [Mn(acac)$_3$] (E_{pc} > 0.56 V). The observed pattern was highlighted for all oxygenated captodative ligands and some sulfur homologues. Conversely, the few sulfur captodative ligands that negatively affect the kinetics of polymerization have a cathodic peak potential that is much lower than that of the initial complex (E_{pc} ≪ 0.56 V). In conclusion, the narrow redox potential window for which manganese complexes reflect the possibility of improving the redox polymerization of Elium® was established and could be used in the near future to fine-tune redox potentials *via* ligand modifications.

Conflicts of interest

There are no conflicts to declare.

Acknowledgements

The authors thank the Agence Nationale de la Recherche (ANR) for the funding of this work (project: ANR-19-CE07-0042).

References

1 K. M. F. Hasan, P. G. Horváth and T. Alpár, Potential Fabric-Reinforced Composites: A Comprehensive Review, *J. Mater. Sci.*, 2021, **56**(26), 14381–14415, DOI: **10.1007/s10853-021-06177-6**.

2 I. Y. Chang and J. K. Lees, Recent Development in Thermoplastic Composites: A Review of Matrix Systems and Processing Methods, *J. Thermoplast. Compos. Mater.*, 1988, **1**(3), 277–296, DOI: **10.1177/089270578800100305**.

3 X. Gabrion, V. Placet, F. Trivaudey and L. Boubakar, About the Thermomechanical Behaviour of a Carbon Fibre Reinforced High-Temperature Thermoplastic Composite, *Composites, Part B*, 2016, **95**, 386–394, DOI: **10.1016/j.compositesb.2016.03.068**.

4 S. K. Bhudolia, G. Gohel, D. Vasudevan, K. F. Leong and P. Gerard, On the Mode II Fracture Toughness, Failure, and Toughening Mechanisms of Wholly Thermoplastic Composites with Ultra-Lightweight Thermoplastic Fabrics and Innovative Elium® Resin, *Composites, Part A*, 2022, **161**, 107115, DOI: **10.1016/j.compositesa.2022.107115**.

5 S. K. Bhudolia, G. Gohel, K. F. Leong and S. C. Joshi, Damping, Impact and Flexural Performance of Novel Carbon/Elium® Thermoplastic Tubular Composites, *Composites, Part B*, 2020, **203**, 108480, DOI: **10.1016/j.compositesb.2020.108480**.

6 W. Obande, C. M. Ó. Brádaigh and D. Ray, Continuous Fibre-Reinforced Thermoplastic Acrylic-Matrix Composites Prepared by Liquid Resin Infusion – A Review, *Composites, Part B*, 2021, **215**, 108771, DOI: **10.1016/j.compositesb.2021.108771**.

7 S. Allagui, A. El Mahi, J.-L. Rebiere, M. Beyaoui, A. Bouguecha and M. Haddar, Effect of Recycling Cycles on the Mechanical and Damping Properties of Flax Fibre Reinforced Elium Composite: Experimental and Numerical Studies, *J. Renewable Mater.*, 2021, **9**(4), 695–721, DOI: **10.32604/jrm.2021.013586**.

8 D. S. Cousins, Y. Suzuki, R. E. Murray, J. R. Samaniuk and A. P. Stebner, Recycling Glass Fiber Thermoplastic Composites from Wind Turbine Blades, *J. Cleaner Prod.*, 2019, **209**, 1252–1263, DOI: **10.1016/j.jclepro.2018.10.286**.

9 H. Bel Haj Frej, R. Léger, D. Perrin, P. Ienny, P. Gérard and J.-F. Devaux, Recovery and Reuse of Carbon Fibre and Acrylic Resin from Thermoplastic Composites Used in Marine Application, *Resour., Conserv. Recycl.*, 2021, **173**, 105705, DOI: **10.1016/j.resconrec.2021.105705**.

10 R. E. Murray, S. Jenne, D. Snowberg, D. Berry and D. Cousins, Techno-Economic Analysis of a Megawatt-Scale Thermoplastic Resin Wind Turbine Blade, *Renewable*

Energy, 2019, **131**, 111–119, DOI: 10.1016/j.renene.2018.07.032.

11 R. E. Murray, R. Beach, D. Barnes, D. Snowberg, D. Berry, S. Rooney, M. Jenks, B. Gage, T. Boro, S. Wallen and S. Hughes, Structural Validation of a Thermoplastic Composite Wind Turbine Blade with Comparison to a Thermoset Composite Blade, *Renewable Energy*, 2021, **164**, 1100–1107, DOI: 10.1016/j.renene.2020.10.040.

12 M. Le Dot, N. Giacoletto, F. Morlet-Savary, B. Graff, V. Monnier, D. Gigmes, M. Nechab, F. Dumur, P. Gerard and J. Lalevée, Synergistic Approach of Type I Hybrid Complexes for Highly Efficient Metal-Based Initiating Strategies: Toward Low Energy-Consuming Polymerization for Thermoplastic Composite Implementation, *Eur. Polym. J.*, 2023, **186**, 111871, DOI: 10.1016/j.eurpolymj.2023.111871.

13 *Substance Information – ECHA*. https://echa.europa.eu/fr/substance-information/-/substanceinfo/100.071.211 (accessed 2023-06-02).

14 P. Garra, F. Dumur, M. Nechab, F. Morlet-Savary, C. Dietlin, B. Graff, E. P. Doronina, V. F. Sidorkin, D. Gigmes, J.-P. Fouassier and J. Lalevée, Peroxide-Free and Amine-Free Redox Free Radical Polymerization: Metal Acetylacetonates/Stable Carbonyl Compounds for Highly Efficient Synthesis of Composites, *Macromolecules*, 2018, **51**(16), 6395–6404, DOI: 10.1021/acs.macromol.8b01360.

15 J. P. Peterson and A. H. Winter, Solvent Effects on the Stability and Delocalization of Aryl Dicyanomethyl Radicals: The Captodative Effect Revisited, *J. Am. Chem. Soc.*, 2019, **141**(32), 12901–12906, DOI: 10.1021/jacs.9b06576.

16 H. Olleik, C. Nicoletti, M. Lafond, E. Courvoisier-Dezord, P. Xue, A. Hijazi, E. Baydoun, J. Perrier and M. Maresca, Comparative Structure–Activity Analysis of the Antimicrobial Activity, Cytotoxicity, and Mechanism of Action of the Fungal Cyclohexadepsipeptides Enniatins and Beauvericin, *Toxins*, 2019, **11**(9), 514, DOI: 10.3390/toxins11090514.

17 H. W. Choi, M. Tian, F. Song, E. Venereau, A. Preti, S.-W. Park, K. Hamilton, G. V. T. Swapna, M. Manohar, M. Moreau, A. Agresti, A. Gorzanelli, F. De Marchis, H. Wang, M. Antonyak, R. J. Micikas, D. R. Gentile, R. A. Cerione, F. C. Schroeder, G. T. Montelione, M. E. Bianchi and D. F. Klessig, Aspirin's Active Metabolite Salicylic Acid Targets High Mobility Group Box 1 to Modulate Inflammatory Responses, *Mol. Med.*, 2015, **21**(1), 526–535, DOI: 10.2119/molmed.2015.00148.

18 H. Jean Nono, D. Bikélé Mama, J. N. Ghogomu and E. Younang, A DFT Study of Structural and Bonding Properties of Complexes Obtained from First-Row Transition Metal Chelation by 3-Alkyl-4-Phenylacetylamino-4,5-Dihydro-1H-1,2,4-Triazol-5-One and Its Derivatives, *Bioinorg. Chem. Appl.*, 2017, **2017**, 1–15, DOI: 10.1155/2017/5237865.

19 Y. Yu, Y. Feng, R. Chauvin, S. Ma, L. Wang and X. Cui, One-Pot Access to *Peri* -Condensed Heterocycles via Manganese-Catalyzed Cascade C–N and C–C Bond Formation, *Org. Lett.*, 2018, **20**(14), 4209–4212, DOI: 10.1021/acs.orglett.8b01586.

20 R. Das, K. R. Rohit and G. Anilkumar, Recent Trends in Non-Noble Metal-Catalyzed Hydroxylation Reactions, *J. Organomet. Chem.*, 2022, **977**, 122456, DOI: 10.1016/j.jorganchem.2022.122456.

21 P. A. Vigato, V. Peruzzo and S. Tamburini, The Evolution of β-Diketone or β-Diketophenol Ligands and Related Complexes, *Coord. Chem. Rev.*, 2009, **253**(7–8), 1099–1201, DOI: 10.1016/j.ccr.2008.07.013.

22 R. Lomoth, P. Huang, J. Zheng, L. Sun, L. Hammarström, B. Åkermark and S. Styring, Synthesis and Characterization of a Dinuclear Manganese(III,III) Complex with Three Phenolate Ligands, *Eur. J. Inorg. Chem.*, 2002, **2002**(11), 2965–2974, DOI: 10.1002/1099-0682(200211)2002:11<2965::AID-EJIC2965>3.0.CO;2-3.

23 T. Nakamura, K. Niwa, S. Usugi, H. Asada, M. Fujiwara and T. Matsushita, Novel Dinuclear Manganese(III) Complexes with Bi- or Tridentate and Bridging Tetradentate Schiff Base Ligands: Preparation, Properties and Catalase-like Function, *Polyhedron*, 2001, **20**(3–4), 191–201, DOI: 10.1016/S0277-5387(00)00636-7.

24 C. Palopoli, J. Ferreyra, A. Conte-Daban, M. Richezzi, A. Foi, F. Doctorovich, E. Anxolabéhère-Mallart, C. Hureau and S. R. Signorella, Insights into Second-Sphere Effects on Redox Potentials, Spectroscopic Properties, and Superoxide Dismutase Activity of Manganese Complexes with Schiff-Base Ligands, *ACS Omega*, 2019, **4**(1), 48–57, DOI: 10.1021/acsomega.8b03018.

25 M. Sjödin, J. Gätjens, L. C. Tabares, P. Thuéry, V. L. Pecoraro and S. Un, Tuning the Redox Properties of Manganese(II) and Its Implications to the Electrochemistry of Manganese and Iron Superoxide Dismutases, *Inorg. Chem.*, 2008, **47**(7), 2897–2908, DOI: 10.1021/ic702428s.

26 W. M. Coleman, R. R. Goehring, L. T. Taylor, J. G. Mason and R. K. Boggess, Electrochemical Studies on a Series of Manganese(III) Complexes Containing Symmetrical Pentadentate Ligands, *J. Am. Chem. Soc.*, 1979, **101**(9), 2311–2315, DOI: 10.1021/ja00503a011.

27 D. P. Kessissoglou, Homo- and Mixed-Valence EPR -Active Trinuclear Manganese Complexes, *Coord. Chem. Rev.*, 1999, **185–186**, 837–858, DOI: 10.1016/S0010-8545(99)00040-5.

